Journal of
Cell Science
Volume 116 (20) October 15, 2003

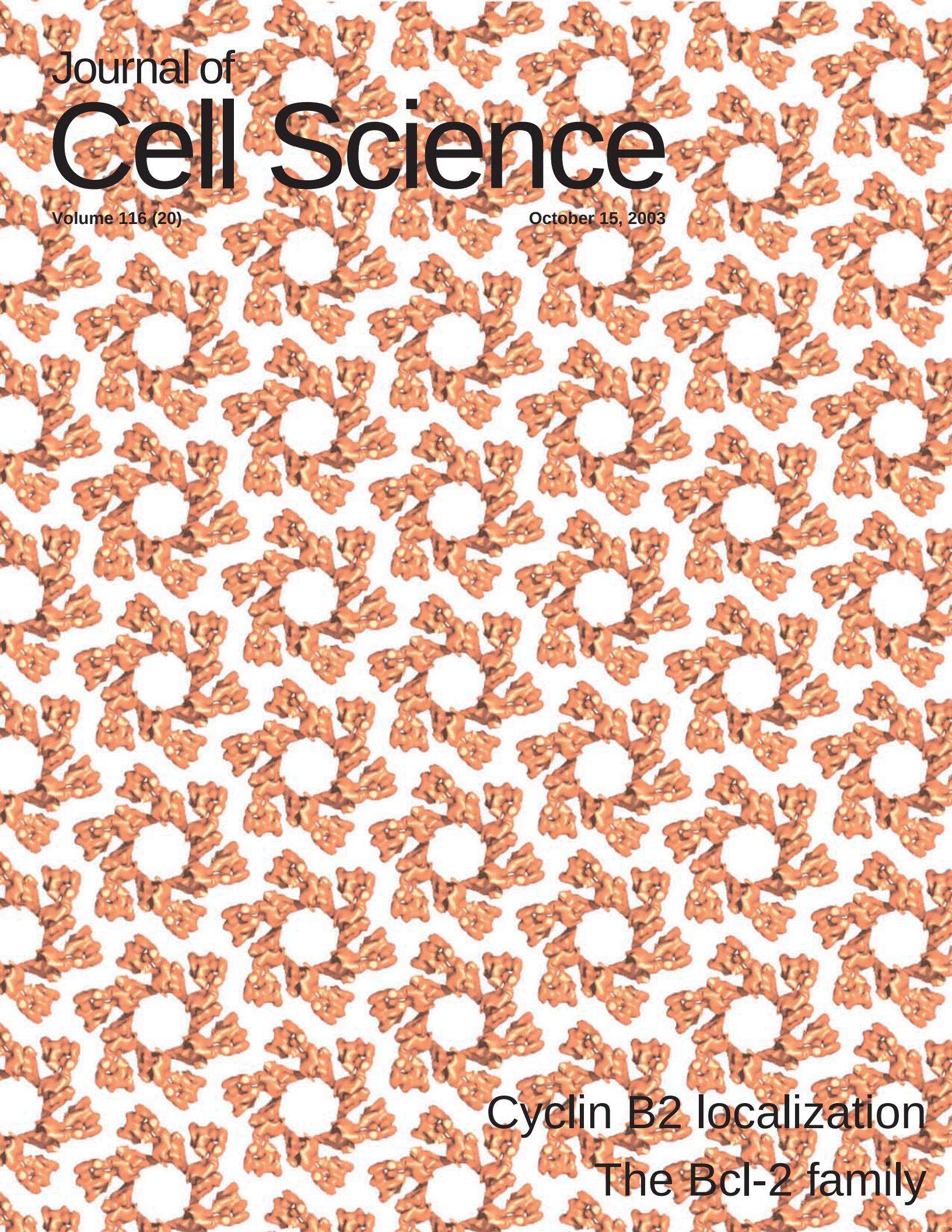

Cyclin B2 localization

The Bcl-2 family

Structural basis of urothelial permeability barrier function as revealed by Cryo-EM studies of the 16 nm uroplakin particle

Guangwei Min[1], Ge Zhou[1], Matthieu Schapira[1], Tung-Tien Sun[2] and Xiang-Peng Kong[1,*]

[1]Structural Biology Program, Skirball Institute of Biomolecular Medicine, Departments of [1]Biochemistry, [2]Dermatology, [2]Pharmacology and [2]Urology, [2]Kaplan Comprehensive Cancer Center, New York University School of Medicine, New York, NY 10016, USA

*Author for correspondence (e-mail: kong@saturn.med.nyu.edu)

Accepted 20 June 2003
Journal of Cell Science 116, 4087-4094 © 2003 The Company of Biologists Ltd
doi:10.1242/jcs.00811

Summary

The apical surface of terminally differentiated mammalian urothelial umbrella cells is covered by numerous plaques consisting of two-dimensional (2D) crystals of hexagonally packed 16 nm uroplakin particles, and functions as a remarkable permeability barrier. To determine the structural basis of this barrier function, we generated, by electron cryo microscopy, a projection map of the isolated mouse urothelial plaques at 7 Å and a 3D structure at 10 Å resolution. Our results indicate that each 16 nm particle has a central 6 nm lipid-filled 'hole' surrounded by 6 inverted U-shaped subunits, each consisting of an inner and an outer subdomain connected via a distal joint. The transmembrane portion of each subdomain can fit about 5 helices. This finding, coupled with our STEM and EM data, suggests that uroplakin pairs Ia/II and Ib/III are associated with the inner and outer subdomains, respectively. Since the inner subdomains interconnect to form a ring, which can potentially segregate the lipids of the central hole from those outside, the 2D crystalline uroplakin network may impose an organized state and a severely restricted freedom of movement on the lipid components, thus reducing membrane fluidity and contributing to the barrier function of urothelial plaques. Our finding that distinct uroplakin substructures are in contact with the cytoplasmic and exoplasmic leaflets of the plaque suggests that the two leaflets may have different lipid composition and contribute asymmetrically to the barrier function. We propose that the crystalline lattice structure of uroplakin, through its interactions with specialized lipids, plays a major role in the remarkable permeability barrier function of urothelial apical surface. Our results also have implications for the transmembrane signal transduction in urothelial cells as induced by the binding of uropathogenic *E. coli* to its uroplakin receptor.

Key words: Urothelium, Uroplakin, Electron cryo-microscopy, Plasma membrane, Permeability barrier, Tetraspanin

Introduction

A striking feature of the mammalian urothelial apical surface is that it is almost entirely covered by rigid-looking plaques (also known as the asymmetric unit membrane or AUM) consisting of 16 nm uroplakin (UP) particles that naturally form two-dimensional (2D) crystals and are interconnected by relatively particle-free 'hinge' areas (Koss, 1969; Staehelin et al., 1972; Hicks, 1975; Lewis, 2000). Urothelial apical membrane therefore provides an attractive system for studying membrane assembly, regulation and function. Moreover, the urothelial apical surface plays several important roles in urothelial function and diseases. First, mammalian bladder epithelium has evolved to be one of the most efficient permeability barriers known to exist in nature, capable of maintaining a steep concentration gradient of solutes between the urine and plasma (Hicks, 1975; Chang et al., 1994; Negrete et al., 1996a; Lewis, 2000). Although the apical surface of the urothelium has been determined to be the site of the permeability barrier for urea, ammonium and other small non-electrolytes (Negrete et al., 1996a), the structural basis for this permeability barrier function is unclear. Second, it is thought that urothelial plaques can be retracted into the cytoplasm forming fusiform vesicles during bladder contraction, and be re-inserted into the apical surface during bladder distention thus achieving a reversible adjustment of apical urothelial surface area (Porter et al., 1967; Minsky and Chlapowski, 1978; Lewis and de Moura, 1982). The mechanism of this process is, however, not well understood. Third, uroplakin Ia has been shown to be the urothelial receptor for type 1-fimbriated *E. coli* (Wu et al., 1996; Zhou et al., 2001; Min et al., 2002), which causes the majority of urinary tract infections (Hagberg et al., 1981; Svanborg and de Man, 1987; Johnson, 1991; Hooton and Stamm, 1997; Langermann et al., 1997). The binding of such uropathogenic bacteria to a urothelial surface receptor can trigger urothelial apoptosis, as well as the urothelial engulfment of the bacteria leading to intra-urothelial bacterial survival and replication (Mulvey et al., 1998; Mulvey et al., 2000). These intra-urothelial bacteria may play a role in recurrent urinary tract infection (Mulvey et al., 2000; Schilling and Hultgren, 2002). Little is known, however, about the structural mechanism by which the binding of the bacteria to an extracellular domain of the uroplakin receptor can trigger the cytoplasmic signal transduction cascades culminating in urothelial changes and bacteria invasion.

Highly purified bovine urothelial plaques contain four major uroplakins (UPs), i.e., UP Ia (27 kDa), Ib (28 kDa), II (15 kDa) and III (47 kDa), which have been conserved during mammalian evolution (Wu et al., 1990; Yu et al., 1990; Wu and Sun, 1993; Lin et al., 1994; Wu et al., 1994; Yu et al., 1994). The closely related UP Ia and Ib have four transmembrane domains connecting one large and one small luminal loop, and belong to the 'tetraspanin' family (Yu et al., 1994; Hemler, 2001). Members of this family include CD9, CD81, CD82 and CD151, which interact with integrins, B cell receptor and other signaling membrane proteins, and play roles in cell adhesion, cell motility and growth regulation (for reviews, see Maecker et al., 1997; Boucheix and Rubinstein, 2001; Hemler, 2001). UP Ia and Ib interact preferentially with UP II and III, respectively (Wu et al., 1995; Liang et al., 2001; Tu et al., 2002). With the exception of uroplakin III that has a relatively long cytoplasmic domain of about 50 amino acids, the three other uroplakins have extremely small cytoplasmic domains. It has been suggested that the extracellular domains of uroplakins interact tightly with one another forming the extracellular portion of the 16 nm particle characteristic of the urothelial apical surface, while the cytoplasmic tail of uroplakin III is somehow involved in mediating membrane-cytoskeletal interaction (Yu et al., 1994).

Studies of negatively stained urothelial plaques by electron microscopy (EM) coupled with image processing showed that each 16 nm urothelial plaque particle consists of 6 inner and 6 outer subdomains interconnected to form a 'twisted ribbon-like' structure (Hicks and Ketterer, 1969; Vergara et al., 1969; Brisson and Wade, 1983; Taylor and Robertson, 1984; Walz et al., 1995; Min et al., 2002). The lipid-embedded domain of the 16 nm particle was visualized by freeze fracture and electron cryo microscopy (cryo-EM), which revealed a transmembrane structure penetrating the lipid bilayer (Staehelin et al., 1972; Kachar et al., 1999; Oostergetel et al., 2001). Although earlier EM studies suggested that the cytoplasmic side of the plaque was smooth, atomic force microscopy studies revealed circular protrusions on the cytoplasmic surface of urothelial plaques (Min et al., 2002), consistent with the current understanding that all uroplakin subunits are integral membrane proteins (Yu et al., 1994; Sun et al., 1999).

To better understand the biological functions of urothelial plaques, we have determined the three-dimensional (3D) structure of mouse urothelial 16 nm particles to 10 Å resolution using electron cryo microscopy, which allows the visualization of the entire uroplakin particle including its transmembrane domains. Our results enabled us to construct a urothelial plaque model suggesting the association of individual uroplakin pairs with specific subdomains of the 16 nm particle, and a possible structural basis of urothelial permeability barrier function.

Materials and Methods

Isolation of urothelial plaques and cryo-EM sample preparation

Mouse urothelial plaques were isolated using improved procedures of sucrose density gradient centrifugation coupled with differential detergent wash (Wu et al., 1990; Liang et al., 1999) (Fig. 1A,B). For cryo-EM study, we used a back-injection method for grid preparation (Wang and Kuhlbrandt, 1991). 5 μl of purified urothelial plaques (0.1 mg/ml in 15 mM Hepes-NaOH (pH 7.5), 1 mM EDTA and 1 mM EGTA) were adsorbed to carbon films on molybdenum grids (300 meshes; Electron Microscopy Science, Fort Washington, PA) with a drop of 0.75% tannic acid (pH 6.0). After the excess liquid was blotted with filter paper, the grid was quickly plunged into liquid nitrogen and transferred, at the liquid nitrogen temperature, to a Gatan cryo-holder. Electron micrographs were recorded using a Philips CM200 FEG electron microscope operated at 200 kV.

Image recording and processing

Micrographs were taken at a magnification of 50,000× under low-dose conditions: only those urothelial plaques greater than 0.5 μm in diameter were imaged. After each exposure, the urothelial plaque was examined using a CCD camera to ensure that the plaque was single layered. For 3D reconstruction, images of up to 50° tilt angle were taken. For image processing, the micrographs were first screened by optical diffraction to select the best regions that yielded the highest resolution diffractions. Micrographs with diffraction spots no higher than 15 Å resolution were discarded. The selected electron micrographs were then digitized using a ZEISS SCAI scanner at a step size of 14 μm, which corresponded to 2.8 Å in the crystal. A total of 45 images were corrected for long-range disorder, merged, averaged and the 3D density map was calculated (only structural factors up to 10 Å resolution were included) using MRC and CCP4 software suites (Henderson et al., 1990; CCP4, 1994; Crowther et al., 1996). The density map was visualized using program O (Jones et al., 1991) and the figures were rendered with Pov-Ray. Portions of this work have been reported previously in an abstract at the 41st American Society for Cell Biology Annual Meeting, in December 2001, in Washington, DC.

Results and Discussion

To study the 3D structure of the 16 nm uroplakin particle (Fig. 1A and B show the transmission EM structure of mouse urothelial apical surface and a negatively stained mouse urothelial plaque, respectively), we recorded a tilted series of images of frozen-hydrated, purified mouse urothelial plaques. Collection of data using large urothelial plaques with a diameter of up to ~1 μm enabled us to calculate diffractions up to 7 Å in resolution under low dose conditions (Fig. 1C). This enabled us to obtain a 2D projection map at 7 Å resolution (Fig. 2), as well as a 3D structure of the mouse uroplakin particle at 10 Å resolution in the membrane plane and 16.5 Å in the vertical direction (Table 1; Figs 3 and 4). While the overall shape of our 3D structure was consistent with earlier lower resolution data showing 6 inner and 6 outer subdomains interconnected to form a hexagonal particle (Figs 2 and 4A) (Hicks and Ketterer, 1969; Vergara et al., 1969; Brisson and Wade, 1983; Taylor and Robertson, 1984; Walz et al., 1995; Oostergetel et al., 2001; Min et al., 2002), our 3D map revealed much more structural details. For example, while in a previous model (Oostergetel et al., 2001) the 'joint' connecting the tips of the inner and outer subdomains within a 'subunit' was not well resolved, our reconstruction resolved this connection into multiple strands (Fig. 4A,D). While all the subdomains in previous models appeared solid, our reconstruction revealed the possible presence of a tunnel traversing the entire outer subdomain as seen in both 2D projections (Fig. 2) and 3D maps (Fig. 5). Finally, while the subunits in previous models appeared to be extensively connected, our higher resolution structure showed that the subunits were actually joined via a single, thin connection – even when the density was contoured at 1σ level (Fig. 4E and Fig. 5F, and data not shown).

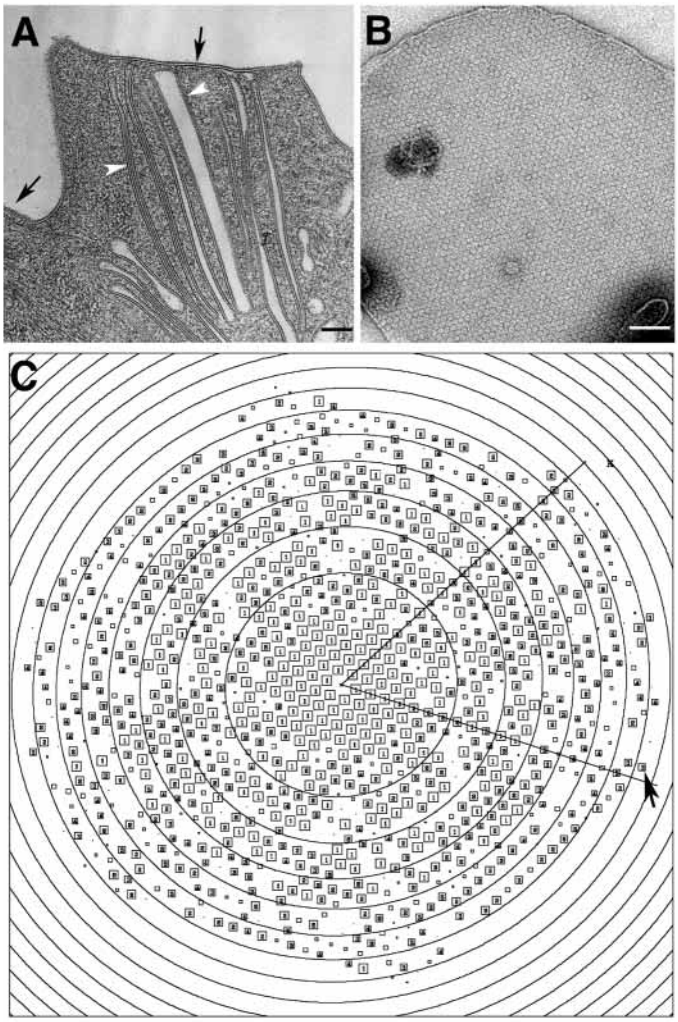

Fig. 1. Mouse urothelial plaques. (A) Concave urothelial plaques make up almost the entire mouse urothelial apical surface (arrows) as well as large cytoplasmic fusiform vesicles (arrowheads). Scale bar: 100 nm. (B) A negatively stained, isolated mouse urothelial plaque showing a crystalline hexagonal array of 16 nm uroplakin particles. Scale bar: 100 nm. (C) The calculated diffraction pattern of a frozen-hydrated mouse urothelial plaque. Each spot with a signal/noise ratio of >1 is shown as a square; the size of the square is proportional to its signal/noise ratio. The number in each square is the 'IQ' number of the diffraction spot [IQ of 1 to 7 correspond to signal-to-noise ratio of 7 to 1, respectively (Henderson et al., 1990)]. Circles are drawn at contrast transfer function (CTF) correction zeros; one spot at 6.9 Å (IQ=3) resolution is marked with an arrow.

Dimension and architecture of the 16 nm particle

When viewed from the side, the 16 nm particle could be divided into four zones (Fig. 4C): the bottom cytoplasmic zone (C), the transmembrane zone (TM), the trunk zone (TK), and the top joint zone (J). We determined the total height of the urothelial particle to be ~12 nm, which is consistent with previously reported values of 12-13 nm based on thin-section electron microscopy (Staehelin et al., 1972; Hicks et al., 1974; Robertson and Vergara, 1980), 13.2 nm based on cryo-EM (Oostergetel et al., 2001), and 12.5 nm based on atomic force microscopy (Min et al., 2002) (unpublished data). Our recent atomic force microscopy data indicated that the extracellular portion of the urothelial particle is 6.5 nm in height (Min et al., 2002) (Fig. 4C). This value also compares favorably with reported values of 5 nm (Brisson and Wade, 1983; Walz et al., 1995) or 5.7 nm based on 3D reconstruction of negatively stained images (Taylor and Robertson, 1984); or 6 nm (Hicks et al., 1974) or 6.5 nm (Robertson and Vergara, 1980) based on thin-section electron microscopy. Finally, our atomic force microscopy data indicate that there is a cytoplasmic protrusion of 0.5 nm (Min et al., 2002). Taken together, these data suggest an ~5 nm transmembrane domain (Fig. 4C), which is considerably thicker than an ordinary phospholipid-type lipid bilayer [usually ~3.5-4 nm (van Meer and Lisman, 2002)]. However, this thickness is consistent with a lipid bilayer of sphingolipids [usually 4.5-5.5 nm (van Meer and Lisman, 2002)], which are known to be enriched in urothelial plaques (see below). The assignment of a 5 nm transmembrane domain, as shown in Fig. 4C, puts a constricted zone, which can be seen in Fig. 4C (open arrowhead), below the exoplasmic surface of the lipid bilayer. Whether this constriction should coincide with the exoplasmic surface (i.e., whether the lipid bilayer thickness should be less than the currently assigned 5 nm) so that the narrow neck can serve as a 'hinge' contributing to the

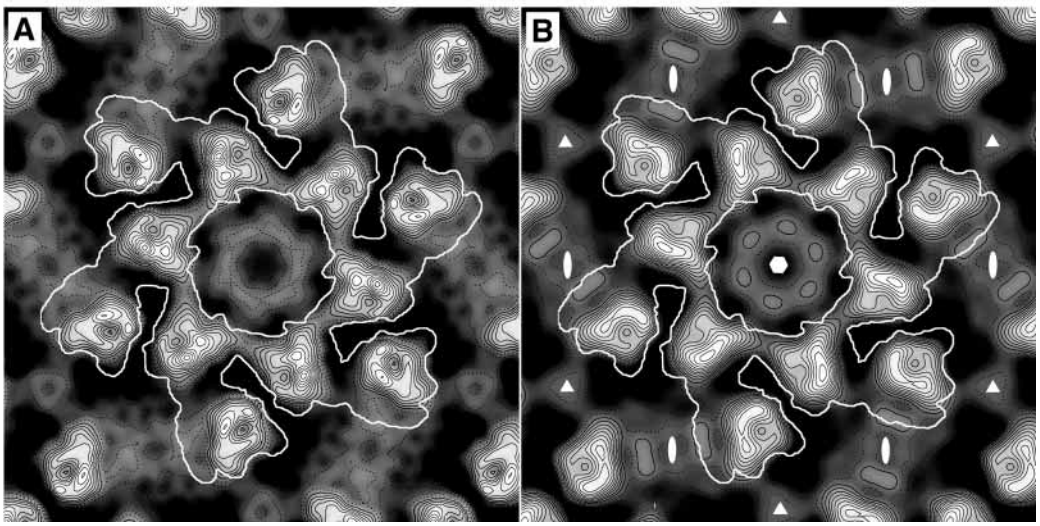

Fig. 2. Projection maps of the mouse urothelial plaque. (A) A map calculated from six untilted crystals, including all data of up to 7 Å resolution. (B) Another projection map calculated using data of up to 12 Å resolution. For comparison, the outlines of the 16 nm particles according to the 3D reconstruction (shown in Fig. 4A) are marked by unbroken white lines; the symmetry elements of twofold (ovals), threefold (triangles) and sixfold (central hexagon) axes are indicated.

Table 1. Summary of the Cry-EM 3D data analysis

Two-side plane group	p6
Unit cell dimension	a=b=16.5±0.2 nm; γ=120°
IQ cut-off* of data	≤7
Number of observed amplitudes/phases	8793
Overall R-factor (%)	36.6
Overall phase residual (90° is random)	36.1°
Weighted phase residual (90° is random)	24.2° (100-10 Å) 24.2° (100-14 Å) 23.1° (14-10 Å)
In-plane resolution	10.0 Å
Estimated resolution normal to the membrane†	16.5 Å
Maximum tilt angle	50°

*Nomenclature of Henderson et al., 1990.
†Based on calculation of point-spread function for the experimental map (Unger and Schertler, 1995).

recently observed flexibility of the urothelial particle (Kachar et al., 1999) needs to be further studied.

Each outer subdomain was connected to the closest neighboring inner subdomain at the top via a horizontal 'joint' (Fig. 4A,D), forming one of the six inverted U-shaped 'subunits' (for a top view of a subunit outlined in blue see Fig. 4A; for side view see Fig. 4D), which most likely represent the basic building blocks of the 16 nm particle (Warren and Hicks, 1978). However, the inner subdomain of each subunit formed relatively thin contacts with the inner subdomains of the two neighboring subunits (Fig. 4E; double arrowhead). The transmembrane zones of both inner and outer subdomains were cylindrical in shape, and were both nearly perpendicular to the membrane plane (Fig. 4C-E).

Different levels of subdomain and subunit interactions

As mentioned earlier, uroplakins Ia and Ib belong to the tetraspanin gene family (Yu et al., 1994; Maecker et al., 1997; Boucheix and Rubinstein, 2001; Hemler, 2001). Many tetraspanin proteins can form networks (or 'webs') on the cell surface by interacting with other tetraspanins as well as some single transmembrane-domained proteins involved in signal transduction (Boucheix and Rubinstein, 2001). With the exception of CD81 whose large extracellular loop has been solved to atomic resolution (Kitadokoro et al., 2001), relatively little is known about the structure of tetraspanin complexes. Thus structural analysis of uroplakin tetraspanin complexes that naturally form 2D crystals provides a unique opportunity to better understand how tetraspanins interact with each other and with other single transmembrane-domained integral membrane proteins.

Our data indicate that there are probably four levels of interactions involved in the formation of a crystalline uroplakin network. (i) The first level of interaction involves the association of the tetraspanin uroplakins Ia and Ib with their partner uroplakins II and III, respectively, to form a heterodimer (Wu et al., 1995; Liang et al., 2001; Tu et al., 2002). As will be discussed later, available EM localization and STEM data suggest that UPIa/II and UPIb/III uroplakin pairs are associated with the inner and outer subdomains, respectively (Fig. 5J). Within each subdomain, the two members of the uroplakin pair appear to interact through both their extracellular and transmembrane domains (Fig. 4D,E, Fig. 5I,J). (ii) In the next level of interaction, the tip of each inner subdomain is connected to that of a neighboring outer subdomain through an extracellular 'joint' to form an inverted U-shaped subunit (Fig. 4D). The joint probably consists of mainly the N-terminal moieties of the single transmembrane-domained uroplakins, i.e., UPII and UPIII, because the joint occupies the top 3 nm of the 12 nm tall particle, but even the larger extracellular loop of UP Ia and Ib extents to only about 9 nm (including the transmembrane domains) according to structural modeling (data not shown) [see also Bienstock and Barrett (Bienstock and Barrett, 2001) for the structural model of CD82, another tetraspanin also known as KAI-1]. (iii) On the next level, each inverted U-shaped subunit is associated with its neighboring subunit via a small connection located below the exoplasmic leaflet of the lipid bilayer (Fig. 4A,E; double arrowhead); these small connections link the 6 subunits together to form a 16 nm particle (Fig. 4A). Although these inter-subunit connections seem much less extensive when compared with the inter-subdomain interactions mediated by the joint, they appear to form a complete ring that can potentially hinder the intermixing of lipids located in the central hole and those in the interparticle region (see below). (iv) Finally, the 16 nm particles are packed hexagonally to form a crystalline plaque (Fig. 4B). This inter-particle interaction

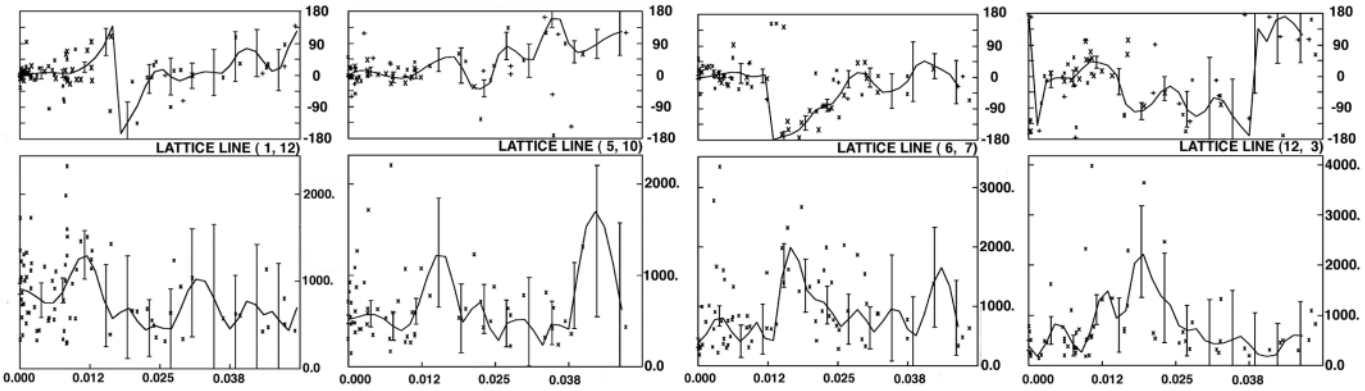

Fig. 3. The phase and amplitude variations along some of the high resolution lattice lines. The data points included all the spots with IQ<6 after merging all the data from the tilt series. The fitting curves were computed using the LATLINE program from the MRC software suite (Agard, 1983).

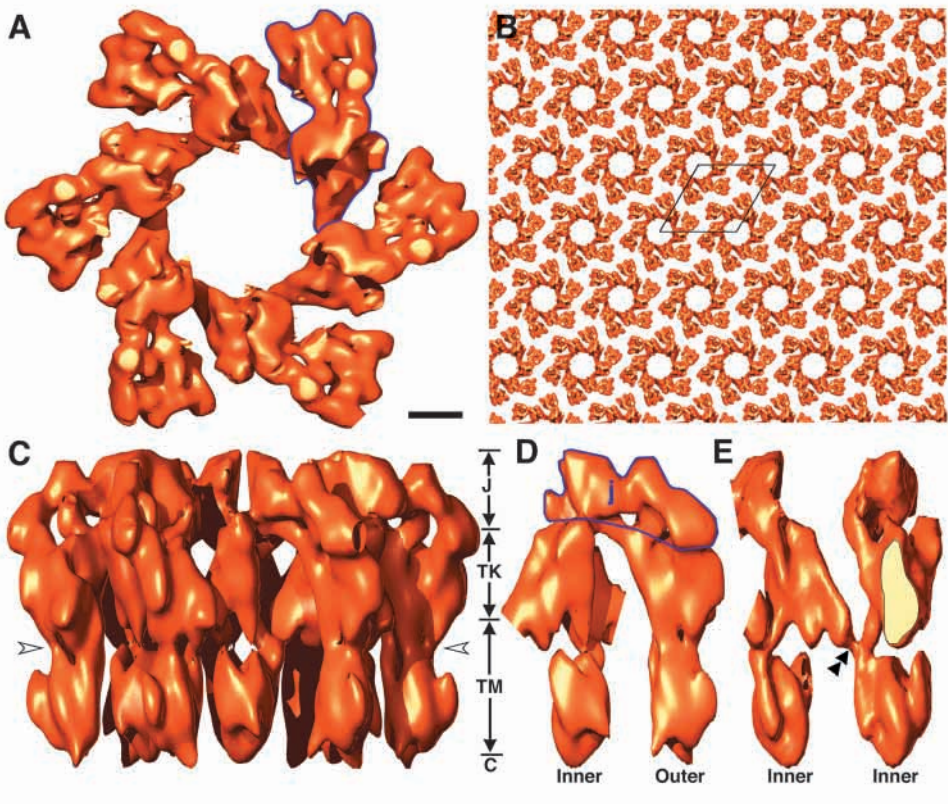

Fig. 4. The 3D structure of the 16 nm mouse uroplakin particle at 10 Å resolution. (A) The top view of the 3D density map of a mouse 16 nm uroplakin particle that is contoured at the 1.5σ level. The boundary of a 'subunit' consisting of an inner and an outer subdomain is outlined in blue. (B) The particles as seen in a hexagonal crystalline array with one unit cell illustrated. (C) The side view of the 16 nm particle showing, from top to bottom, the joint (J), trunk region (TK), transmembrane domain (TM) and cytoplasmic domain (C). (D) One of the six inverted U-shaped subunits of the 16 nm particle, consisting of an inner subdomain (left) connected to an outer (right) subdomain via a (top) horizontal joint (j; outlined in blue). This inverted U-shaped subunit presumably represents a fundamental building block of the 16 nm particle (Staehelin et al., 1972; Hicks et al., 1974). (E) The inner subdomains of two neighboring subunits are connected via a minimal contact between them (double arrowhead). In A, the stellate-shaped particle has a maximal diameter of 17.5 nm and has a large lipid-filled, central hole (~6 nm in diameter); in C the particle is about 12 nm tall with a 6.5 nm extracellular and a 0.5 nm cytoplasmic region [from atomic force microscopy data (Min et al., 2002)]. All panels except B are to the same scale; bar (in A) 2 nm. The unit cell in B is 16.5 nm in length.

appears to occur at the 2-fold axes (Fig. 2), consistent with earlier suggestions by Walz et al. (Walz et al., 1995) and Kachar et al. (Kachar et al., 1999). Overall, these considerations suggest that the interactions between the uroplakins to form a subdomain is probably quite extensive; the interactions between the inner and outer subdomains within a subunit are moderately extensive, while the inter-subunit and inter-particle interactions are less extensive (Figs 4 and 5).

A possible tunnel

The density map of the 16 nm particle contoured at level 1.5σ revealed the possible existence of a transmembrane tunnel in the outer subdomain (arrowheads in Fig. 5). Although the inner subdomain appeared to also have a tunnel, it did not traverse the entire height of the subdomain at the 1.5σ contour level. The outer subdomain tunnel had an extracellular opening located at the junction between the top 'joint' and the 'trunk' (arrowheads in Fig. 5B), and an intracellular opening located in the 'cytoplasmic zone' (Fig. 5B,E-H). These two openings were relatively narrow but they led to a chamber in the center of the trunk zone (Fig. 5B). The possible existence of a transmembrane tunnel through the urothelial plaque particle, and its functional implications need to be further investigated.

Uroplakin-lipid interaction as a possible mechanism for the permeability barrier function of urothelial plaque

As mentioned earlier, a key issue in urothelial biology is the structural basis for the extraordinary permeability barrier of urothelial plaques. It seems likely that several factors contribute to this barrier function. First, an interesting feature of the uroplakin particle is the presence of a large central 'hole' (Fig. 4A,B). Although previous negative staining data could not rule out the possible existence of a stain-excluding region in the center of this hole (Taylor and Robertson, 1984; Walz et al., 1995), our cryo-EM data clearly established the absence of protein mass in this area (see also Oostergetel et al., 2001). This means that, despite a prominent protein lattice appearance, the bulk of the plaque surface (~62%) is occupied by lipids (Fig. 4) (see also Hicks et al., 1974). In this regard, it is interesting to note that the lipids of highly purified urothelial plaques (that have not been treated with detergents) are unusually rich in sphingolipids and cholesterol (Vergara et al., 1974; Stubbs et al., 1979; Hu et al., 2002), which favor an ordered lipid structure and possibly microdomain formation (Simons and van Meer, 1988; Simons and Ikonen, 1997; Brown and London, 2000). Second, and importantly, our finding that the six inner subdomains of the 16 nm particle are interconnected to form a complete ring that is located either slightly below, or coincide with, the exoplasmic surface (Fig. 4E and Fig. 5F) raises the possibility that the lipids of the exoplasmic surface may be physically segregated, thus further enhancing the formation of various lipid microdomains. Third, the crystalline lattice of uroplakin proteins may promote an organized state and impose structural constraints on the freedom of movement of the lipid molecules thus greatly reducing membrane fluidity, which has been shown to correlate with the membrane permeability to water and other solutes (Lande et al., 1995). We therefore propose that the crystalline

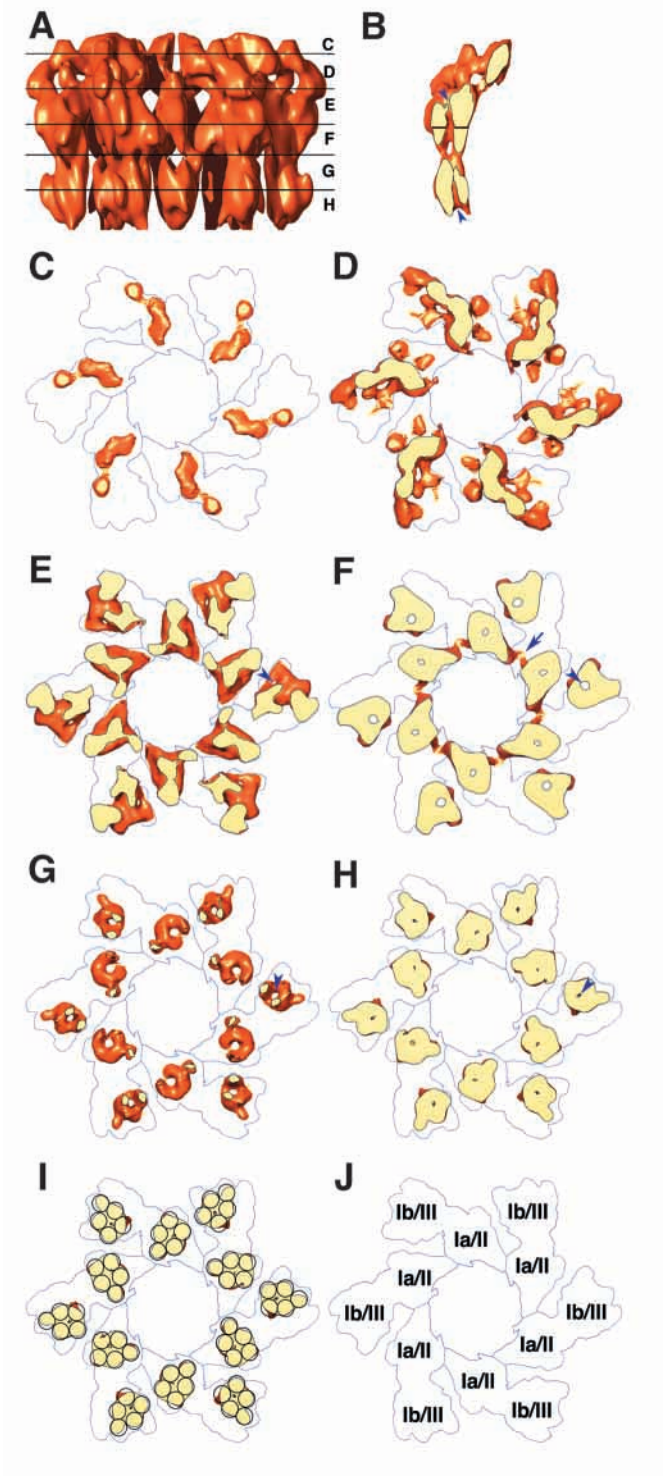

Fig. 5. Cross-sections of the 16 nm mouse uroplakin particle and placement of the transmembrane helices. (A) A 16 nm particle with the positions of the six sections (~20 Å) shown in C-H (top to bottom) indicated by the horizontal lines. (B) A vertical section of one outer subdomain. A tunnel is present that appears to traverse through the entire outer domain (arrowheads in B,E-H). In F, the minimal link between the inner subdomains of neighboring subunits (arrow). (I) Five transmembrane helices, each represented by a 1 nm circle, can fit in the middle of the transmembrane zone (as shown in H). Although F-H seem to indicate the presence of a tunnel also in the inner subdomain, this tunnel does not appear to traverse through the entire height of the subdomain. (J) Hypothetical assignment of uroplakin pairs Ia/II and Ib/III to the inner and outer subdomains, respectively, of the 16 nm urothelial particle. The outlines of the 16 nm particle are drawn in thin blue lines in C-J.

lattice of the uroplakins, through its interactions with specialized lipids, may play an important role in the formation of the remarkable permeability barrier of urothelial plaques. This conclusion is supported by our recent finding that genetic ablation of the uroplakin III gene results in much smaller plaques [in which UPIII is presumably replaced by its minor isoform IIIb (Deng et al., 2002)] and in compromised functioning of the permeability barrier (Hu et al., 2000).

The uroplakin structure as described here (Fig. 4) also has implications on the possibly asymmetric contributions by the two leaflets of the urothelial plaque to the functioning of the permeability barrier. Zeidel and co-workers have shown that the reconstituted model exoplasmic membrane of MDCK cells is much more effective as a permeability barrier to solutes and ammonia than the reconstituted cytoplasmic membrane (Hill and Zeidel, 2000) suggesting that, in this case, the two leaflets of a membrane bilayer, with different lipid compositions, can function as independent permeability barriers (Negrete et al., 1996b; Hill et al., 1999; Krylov et al., 2001). Our finding that the portions of the uroplakin particle that are in contact with the two leaflets of the urothelial plaque are structurally distinct (Fig. 4C-E) is likely to favor asymmetric lipid composition of the two leaflets, which may contribute differently to the permeability barrier function of the urothelial plaques.

Possible association of uroplakin pairs Ia/II and Ib/III with the inner and outer subdomains, respectively, of the 16 nm particle

A better understanding of urothelial plaque function requires the localization of individual uroplakins. Recent data indicate that the four uroplakins form two pairs consisting of uroplakins Ia/II and Ib/III, based on data from chemical crosslinking (Wu et al., 1995), ion exchanger isolation of heterodimer complexes (Liang et al., 2001), genetic ablation of the uroplakin III gene (Hu et al., 2000) and transient transfection studies (Deng et al., 2002; Tu et al., 2002). With regard to the uroplakin composition of the inner and outer subdomains of the 16 nm particle, STEM measurements indicate a total protein mass of 645 kDa per 16 nm particle, or ~107 kDa of protein per each of the 6 subunits [each in turn contains an inner and an outer subdomain (Walz et al., 1995)]. This number is in excellent agreement with the total mass of the two uroplakin pairs (27 kDa (UPIa) + 15 kDa (UPII) + 28 kDa (UPIb) + 47 kDa (UPIII)=117 kDa). In this regard, it is interesting that the transmembrane zone of each subdomain, as depicted in Fig. 5H, can indeed accommodate about 5 transmembrane helices (one tetraspanin plus one single-transmembrane domained UPII or UPIII; Fig. 5I and data not shown). Since we recently showed that uroplakin Ia is associated with the inner subdomains of the 16 nm particle (Min et al., 2002), these results, taken together, raise the possibility that uroplakin pairs Ia/II and Ib/III are associated with the inner and outer subdomains, respectively (Fig. 5J). Additional localization studies are underway to test this hypothesis.

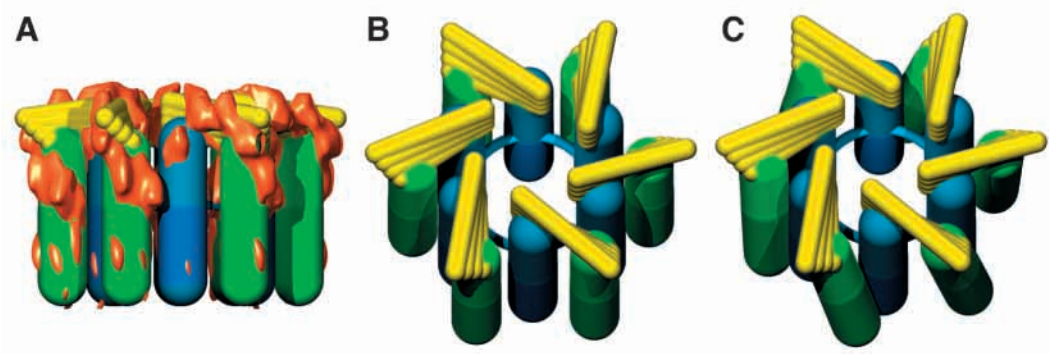

Fig. 6. A schematic model of the 16 nm uroplakin particle. (A) A model in which the inner subdomains, outer subdomains and the joints of the 16 nm urothelial particle are represented by blue cylinders, green cylinders and yellow flexible hinges, respectively. The transmembrane zone is indicated with darker colors. (B) A tilted view of the model. (C) A hypothetical scheme in which the bending of the joint region (yellow) caused by bacterial binding leads to a twist between the inner and outer subdomains; conformational changes such as this may play a role in the transmembrane signal transduction causing urothelial umbrella cells to undergo morphological and physiological changes.

Conformational changes of uroplakin particles and perspectives

Although urothelial plaque has been described as a 'rigid-looking' structure based on its regular, curved appearance in vertical sections by TEM (Fig. 1A), existing data suggest that the 16 nm particle is actually quite flexible and can undergo major conformational changes (Kachar et al., 1999). Consistent with this concept, our data indicate that the uroplakin particle is a remarkably hollow structure (Fig. 4). While each of the 6 inner subdomains is connected to its neighboring outer subdomain at the distal end (top) via a joint (Fig. 4D), relatively little contact exists among the neighboring subunits (Fig. 4E). It would be interesting to determine whether the two subdomains, which are parallel to each other and nearly perpendicular to the membrane, can twist against each other leading to conformational change or movement of the transmembrane domains (Fig. 6). Additional studies of the structure and function of urothelial plaques should shed light on whether such conformational changes can occur and whether such changes play a role in urothelial signal transduction upon bladder stretching and bacterial binding.

We thank Drs Ueli Aebi, Manfred Auer, David Stokes, Da Neng Wang, Howard Young for useful discussions, Juan Lafaille for providing mouse bladder tissues, Rachelle Bienstock for providing the coordinates of modeled CD82, Gert Kreibich and Da Neng Wang for critical reading of the manuscript. We dedicate this paper to Leopold Koss, a pioneer in urothelial research and bladder cancer pathology and cytopathology. This work was supported in part by NIH grants DK52206 (X.P.K. and T.T.S.), DK57269 and DK39753 (T.T.S.).

References

Agard, D. A. (1983). A least-squares method for determining structure factors in three- dimensional tilted-view reconstructions. *J. Mol. Biol.* **167**, 849-852.

Bienstock, R. J. and Barrett, J. C. (2001). KAI1, a prostate metastasis suppressor: prediction of solvated structure and interactions with binding partners; integrins, cadherins, and cell-surface receptor proteins. *Mol. Carcinogen.* **32**, 139-153.

Boucheix, C. and Rubinstein, E. (2001). Tetraspanins. *Cell. Mol. Life Sci.* **58**, 1189-1205.

Brisson, A. and Wade, R. H. (1983). Three-dimensional structure of luminal plasma membrane protein from urinary bladder. *J. Mol. Biol.* **166**, 21-36.

Brown, D. A. and London, E. (2000). Structure and function of sphingolipid- and cholesterol-rich membrane rafts. *J. Biol. Chem.* **275**, 17221-17224.

CCP4 (1994). The CCP4 suite: programs for protein crystallography. *Acta Cryst.* **D50**, 760-763.

Chang, A., Hammond, T. G., Sun, T. T. and Zeidel, M. L. (1994). Permeability properties of the mammalian bladder apical membrane. *Am. J. Physiol.* **267**, C1483-C1492.

Crowther, R. A., Henderson, R. and Smith, J. M. (1996). MRC image processing programs. *J. Struct. Biol.* **116**, 9-16.

Deng, F. M., Liang, F. X., Tu, L., Resing, K. A., Hu, P., Supino, M., Hu, C. C., Zhou, G., Ding, M., Kreibich, G. et al. (2002). Uroplakin IIIb, a urothelial differentiation marker, dimerizes with uroplakin Ib as an early step of urothelial plaque assembly. *J. Cell Biol.* **159**, 685-694.

Hagberg, L., Jodal, U., Korhonen, T. K., Lidin-Janson, G., Lindberg, U. and Svanborg Eden, C. (1981). Adhesion, hemagglutination, and virulence of Escherichia coli causing urinary tract infections. *Infect. Immun.* **31**, 564-570.

Hemler, M. E. (2001). Specific tetraspanin functions. *J. Cell Biol.* **155**, 1103-1108.

Henderson, R., Baldwin, J. M., Ceska, T. A., Zemlin, F., Beckmann, E. and Downing, K. H. (1990). Model for the structure of bacteriorhodopsin based on high-resolution electron cryo-microscopy. *J. Mol. Biol.* **213**, 899-929.

Hicks, R. M. (1975). The mammalian urinary bladder: an accommodating organ. *Biol. Rev. Camb. Philos. Soc.* **50**, 215-246.

Hicks, R. M. and Ketterer, B. (1969). Hexagonal lattice of subunits in the thick luminal membrane of the rat urinary bladder. *Nature* **224**, 1304-1305.

Hicks, R. M., Ketterer, B. and Warren, R. C. (1974). The ultrastructure and chemistry of the luminal plasma membrane of the mammalian urinary bladder: a structure with low permeability to water and ions. *Philos. Trans. R. Soc. London. Ser. B* **268**, 23-38.

Hill, W. G., Rivers, R. L. and Zeidel, M. L. (1999). Role of leaflet asymmetry in the permeability of model biological membranes to protons, solutes, and gases. *J. Gen. Physiol.* **114**, 405-414.

Hill, W. G. and Zeidel, M. L. (2000). Reconstituting the barrier properties of a water-tight epithelial membrane by design of leaflet-specific liposomes. *J. Biol. Chem.* **275**, 30176-30185.

Hooton, T. M. and Stamm, W. E. (1997). Diagnosis and treatment of uncomplicated urinary tract infection. *Infect. Disease Clinics North America* **11**, 551-81.

Hu, P., Deng, F. M., Liang, F. X., Hu, C. M., Auerbach, A. B., Shapiro, E., Wu, X. R., Kachar, B. and Sun, T. T. (2000). Ablation of uroplakin III gene results in small urothelial plaques, urothelial leakage, and vesicoureteral reflux. *J. Cell Biol.* **151**, 961-972.

Hu, P., Meyers, S., Liang, F. X., Deng, F. M., Kachar, B., Zeidel, M. L. and Sun, T. T. (2002). Role of membrane proteins in permeability barrier function: uroplakin ablation elevates urothelial permeability. *Am. J. Physiol. Renal Physiol.* **283**, F1200-F1207.

Johnson, J. R. (1991). Virulence factors in Escherichia coli urinary tract infection. *Clin. Microbiol. Rev.* **4**, 80-128.

Jones, T. A., Zou, J. Y., Cowan, S. W. and Kjeldgaad, M. (1991). Improved methods for building protein models in electron density maps and the location of errors in these models. *Acta Cryst.* **A47**, 110-119.

Kachar, B., Liang, F., Lins, U., Ding, M., Wu, X. R., Stoffler, D., Aebi, U. and Sun, T. T. (1999). Three-dimensional analysis of the 16 nm urothelial plaque particle: luminal surface exposure, preferential head-to-head interaction, and hinge formation. *J. Mol. Biol.* **285**, 595-608.

Kitadokoro, K., Bordo, D., Galli, G., Petracca, R., Falugi, F., Abrignani, S., Grandi, G. and Bolognesi, M. (2001). CD81 extracellular domain 3D

structure: insight into the tetraspanin superfamily structural motifs. *EMBO J.* **20**, 12-18.

Koss, L. G. (1969). The asymmetric unit membranes of the epithelium of the urinary bladder of the rat. An electron microscopic study of a mechanism of epithelial maturation and function. *Lab. Invest.* **21**, 154-168.

Krylov, A. V., Pohl, P., Zeidel, M. L. and Hill, W. G. (2001). Water permeability of asymmetric planar lipid bilayers: leaflets of different composition offer independent and additive resistances to permeation. *J. Gen. Physiol.* **118**, 333-340.

Lande, M. B., Donovan, J. M. and Zeidel, M. L. (1995). The relationship between membrane fluidity and permeabilities to water, solutes, ammonia, and protons. *J. Gen. Physiol.* **106**, 67-84.

Langermann, S., Palaszynski, S., Barnhart, M., Auguste, G., Pinkner, J. S., Burlein, J., Barren, P., Koenig, S., Leath, S., Jones, C. H. et al. (1997). Prevention of mucosal Escherichia coli infection by FimH-adhesin-based systemic vaccination. *Science* **276**, 607-611.

Lewis, S. A. (2000). Everything you wanted to know about the bladder epithelium but were afraid to ask. *Am. J. Physiol. Renal Physiol.* **278**, F867-F874.

Lewis, S. A. and de Moura, J. L. (1982). Incorporation of cytoplasmic vesicles into apical membrane of mammalian urinary bladder epithelium. *Nature* **297**, 685-688.

Liang, F., Kachar, B., Ding, M., Zhai, Z., Wu, X. R. and Sun, T. T. (1999). Urothelial hinge as a highly specialized membrane: detergent- insolubility, urohingin association, and in vitro formation. *Differentiation* **65**, 59-69.

Liang, F. X., Riedel, I., Deng, F. M., Zhou, G., Xu, C., Wu, X. R., Kong, X. P., Moll, R. and Sun, T. T. (2001). Organization of uroplakin subunits: transmembrane topology, pair formation and plaque composition. *Biochem. J.* **355**, 13-18.

Lin, J. H., Wu, X. R., Kreibich, G. and Sun, T. T. (1994). Precursor sequence, processing, and urothelium-specific expression of a major 15-kDa protein subunit of asymmetric unit membrane. *J. Biol. Chem.* **269**, 1775-1784.

Maecker, H. T., Todd, S. C. and Levy, S. (1997). The tetraspanin superfamily: molecular facilitators. *FASEB J.* **11**, 428-442.

Min, G., Stolz, M., Zhou, G., Liang, F., Sebbel, P., Stoffler, D., Glockshuber, R., Sun, T. T., Aebi, U. and Kong, X. P. (2002). Localization of uroplakin Ia, the urothelial receptor for bacterial adhesin FimH, on the six inner domains of the 16 nm urothelial plaque particle. *J. Mol. Biol.* **317**, 697-706.

Minsky, B. D. and Chlapowski, F. J. (1978). Morphometric analysis of the translocation of luminal membrane between cytoplasm and cell surface of transitional epithelial cells during the expansion-contraction cycles of mammalian urinary bladder. *J. Cell Biol.* **77**, 685-697.

Mulvey, M. A., Lopez-Boado, Y. S., Wilson, C. L., Roth, R., Parks, W. C., Heuser, J. and Hultgren, S. J. (1998). Induction and evasion of host defenses by type 1-piliated uropathogenic Escherichia coli. *Science* **282**, 1494-1497.

Mulvey, M. A., Schilling, J. D., Martinez, J. J. and Hultgren, S. J. (2000). From the Cover: Bad bugs and beleaguered bladders: Interplay between uropathogenic Escherichia coli and innate host defenses. *Proc. Natl. Acad. Sci. USA* **97**, 8829-8835.

Negrete, H. O., Lavelle, J. P., Berg, J., Lewis, S. A. and Zeidel, M. L. (1996a). Permeability properties of the intact mammalian bladder epithelium. *Am. J. Physiol.* **271**, F886-F894.

Negrete, H. O., Rivers, R. L., Goughs, A. H., Colombini, M. and Zeidel, M. L. (1996b). Individual leaflets of a membrane bilayer can independently regulate permeability. *J. Biol. Chem.* **271**, 11627-11630.

Oostergetel, G. T., Keegstra, W. and Brisson, A. (2001). Structure of the major membrane protein complex from urinary bladder epithelial cells by cryo-electron crystallography. *J. Mol. Biol.* **314**, 245-252.

Porter, K. R., Kenyon, K. and Badenhausen, S. (1967). Specialization of the unit membrane. *Protoplasma* **63**, 262-274.

Robertson, J. D. and Vergara, J. (1980). Analysis of the structure of intramembrane particles of the mammalian urinary bladder. *J. Cell Biol.* **86**, 514-528.

Schilling, J. D. and Hultgren, S. J. (2002). Recent advances into the pathogenesis of recurrent urinary tract infections: the bladder as a reservoir for uropathogenic Escherichia coli. *Int. J. Antimicrob. Agents* **19**, 457-460.

Simons, K. and Ikonen, E. (1997). Functional rafts in cell membranes. *Nature* **387**, 569-572.

Simons, K. and van Meer, G. (1988). Lipid sorting in epithelial cells. *Biochemistry* **27**, 6197-6202.

Staehelin, L. A., Chlapowski, F. J. and Bonneville, M. A. (1972). Lumenal plasma membrane of the urinary bladder. I. Three-dimensional reconstruction from freeze-etch images. *J. Cell Biol.* **53**, 73-91.

Stubbs, C. D., Ketterer, B. and Hicks, R. M. (1979). The isolation and analysis of the luminal plasma membrane of calf urinary bladder epithelium. *Biochim. Biophys. Acta* **558**, 58-72.

Sun, T. T., Liang, F. X. and Wu, X. R. (1999). Uroplakins as markers of urothelial differentiation. *Adv. Exp. Med. Biol.* **462**, 7-18.

Svanborg, C. and de Man, P. (1987). Bacterial virulence in urinary tract infection. *Infect. Disease Clinics North America* **1**, 731-750.

Taylor, K. A. and Robertson, J. D. (1984). Analysis of the three-dimensional structure of the urinary bladder epithelial cell membranes. *J. Ultrastruct. Res.* **87**, 23-30.

Tu, L., Sun, T. T. and Kreibich, G. (2002). Specific heterodimer formation is a prerequisite for uroplakins to exit from the endoplasmic reticulum. *Mol. Biol. Cell* **13**, 4221-4230.

Unger, V. M. and Schertler, G. F. (1995). Low resolution structure of bovine rhodopsin determined by electron cryo-microscopy. *Biophys. J.* **68**, 1776-1786.

van Meer, G. and Lisman, Q. (2002). Sphingolipid transport: rafts and translocators. *J. Biol. Chem.* **277**, 25855-25858.

Vergara, J., Longley, W. and Robertson, J. D. (1969). A hexagonal arrangement of subunits in membrane of mouse urinary bladder. *J. Mol. Biol.* **46**, 593-596.

Vergara, J., Zambrano, F., Robertson, J. D. and Elrod, H. (1974). Isolation and characterization of luminal membranes from urinary bladder. *J. Cell Biol.* **61**, 83-94.

Walz, T., Haner, M., Wu, X. R., Henn, C., Engel, A., Sun, T. T. and Aebi, U. (1995). Towards the molecular architecture of the asymmetric unit membrane of the mammalian urinary bladder epithelium: a closed "twisted ribbon" structure. *J. Mol. Biol.* **248**, 887-900.

Wang, D. N. and Kuhlbrandt, W. (1991). High-resolution electron crystallography of light-harvesting chlorophyII a/b-protein complex in three different media. *J. Mol. Biol.* **217**, 691-699.

Warren, R. C. and Hicks, R. M. (1978). Chemical dissection and negative staining of the bladder luminal membrane. *J. Ultrastruct. Res.* **64**, 327-340.

Wu, X. R., Lin, J. H., Walz, T., Haner, M., Yu, J., Aebi, U. and Sun, T. T. (1994). Mammalian uroplakins. A group of highly conserved urothelial differentiation-related membrane proteins. *J. Biol. Chem.* **269**, 13716-13724.

Wu, X. R., Manabe, M., Yu, J. and Sun, T. T. (1990). Large scale purification and immunolocalization of bovine uroplakins I, II, and III. Molecular markers of urothelial differentiation. *J. Biol. Chem.* **265**, 19170-19179.

Wu, X. R., Medina, J. J. and Sun, T. T. (1995). Selective interactions of UPIa and UPIb, two members of the transmembrane 4 superfamily, with distinct single transmembrane-domained proteins in differentiated urothelial cells. *J. Biol. Chem.* **270**, 29752-29759.

Wu, X. R. and Sun, T. T. (1993). Molecular cloning of a 47 kDa tissue-specific and differentiation- dependent urothelial cell surface glycoprotein. *J. Cell Sci.* **106**, 31-43.

Wu, X. R., Sun, T. T. and Medina, J. J. (1996). In vitro binding of type 1-fimbriated Escherichia coli to uroplakins Ia and Ib: relation to urinary tract infections. *Proc. Natl. Acad. Sci. USA* **93**, 9630-9635.

Yu, J., Lin, J. H., Wu, X. R. and Sun, T. T. (1994). Uroplakins Ia and Ib, two major differentiation products of bladder epithelium, belong to a family of four transmembrane domain (4TM) proteins. *J. Cell Biol.* **125**, 171-182.

Yu, J., Manabe, M., Wu, X. R., Xu, C., Surya, B. and Sun, T. T. (1990). Uroplakin I: a 27-kD protein associated with the asymmetric unit membrane of mammalian urothelium. *J. Cell Biol.* **111**, 1207-1216.

Zhou, G., Mo, W. J., Min, G. W., Sebbel, P., Neubert, T. A., Glockshuber, R., Wu, X. R., Sun, T. T. and Kong, X. P. (2001). Uroplakin Ia is the urothelial receptor for uropathogenic Escherichia coli: evidence from in vitro FimH binding. *J. Cell Sci.* **114**, 4095-4103.